Supplementary Material for

Waveguide superlattices with artificial gauge field towards colorless and low-crosstalk ultrahigh-density photonic integration

Xuelin Zhang[1], Jiangbing Du[1,], Ke Xu[2], and Zuyuan He[1]*

1 State Key Laboratory of Advanced Optical Communication Systems and Networks, Shanghai Jiao Tong University, 800 Dongchuan Road, Minhang, Shanghai 200240, China

2 Department of Electronic and Information Engineering, Harbin Institute of Technology (Shenzhen), Shenzhen 518055, China

** Corresponding author: dujiangbing@sjtu.edu.cn*

Note 1: Dual-polarization in 800-nm-thick Si_3N_4 waveguide

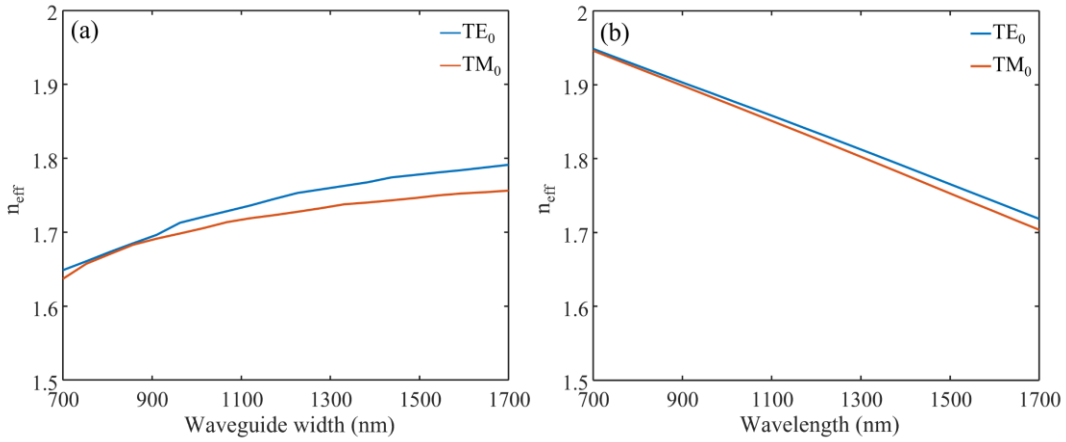

Figure S1 Calculated effective indices of the TE_0 and TM_0 modes of 800-nm-thick waveguides. (a) The effective refractive index of the waveguide width varies from 700 nm to 1700 nm at 1550nm. (b) The effective refractive index of the 1-μm-wide waveguide at a wavelength from 700 nm to 1700 nm.

Low birefringence of silicon nitride waveguides opens up new opportunities for realizing dual-polarization photonic circuits. Fig. S1(a) and (b) show that the effective index for TE_0 mode and TM_0 mode of 800-nm-thick Si_3N_4 waveguide under broadband working bandwidth and waveguide width variation. Due to the geometry of the waveguide and the isotropy of the material, the effective indices are close enough to achieve the dual-polarization dense waveguide array. It can be seen that the effective index for the TE_0 mode is larger than the TM_0 mode because the mode field confinement of the TM_0 mode is weaker than that of the TE_0 mode, and the weak confinement of the

TM_0 mode also enhances the evanescent coupling between the two optical waveguides. With minor refractive index changes for width variation, it indicates that a large propagation constant difference can not be achieved by just choosing different core widths for the optical waveguides, which makes it challenging to implement a densely packed waveguide configuration by directly transplanting existing schemes, which are mostly based on the silicon-on-insulator (SOI) wafer with a large refractive-index contrast.

Note 2: The normal AGF waveguide arrays with GAP = 400 nm

We also simulate the normal AGF waveguide arrays for ease of visual comparison. Fig. S2 shows the transmission spectra of the normal AGF waveguide arrays optimized at 1550 nm, and the results are consistent with those reported in the prior work [16]. This design demonstrates a certain level of crosstalk suppression, but the working bandwidth of $T_{N, N\pm1}$ is very limited, and the crosstalk suppression mechanism is not strong enough, with the peak crosstalk channel surging above − 10 dB at the longer wavelengths. Furthermore, the amplitudes of these uniform sinusoidal curves need to be adjusted with different pitches [16], increasing design complexity and indicating that this method may lack inherent robustness.

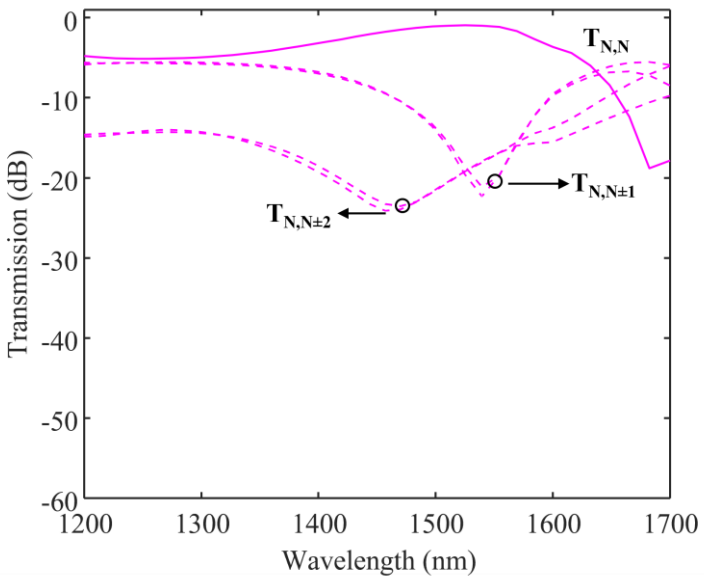

Figure S2 The simulated transmission of the through ($T_{N,N}$), the nearest neighbors ($T_{N,N\pm1}$), and the second nearest neighbors ($T_{N,N\pm2}$) of the normal AGF waveguide array.

Note 3: The modulation period *P*

The modulation period, *P*, is essential for an AGF-enabled superlattice. The modulation period P varying from 15 μm to 35 μm is swept. Specifically, the transmission spectra of the central waveguide in the designed waveguide array alongside its two nearest neighboring waveguides are selected with a gap of 400 nm and length of 200 μm. The influence of the modulation period on the crosstalk can be observed, as depicted in Fig. S3. The results indicate that varying the modulation period from 15 μm to 35 μm induces floating crosstalk between channels, ranging from -10 dB to -32 dB. When P varies between 23 μm and 27 μm, the crosstalk remains <−20-dB, demonstrating the robustness of our approach. The propagation losses increase rapidly with relatively short transmission distances when the P is smaller, reaching 1.5 dB when P = 20 μm and L = 200 μm. It is important to note that light leakage in a bent waveguide follows an exponential function of the number of bends. The reasonable modulation period is related to the inherent material properties; for the silicon-on-insulator (SOI) platform, the modulation period of the AGF waveguide can be as small as 10 μm [16], [17]. Losses incurred by AGF waveguides with smaller modulation periods significantly limit the integration density of PICs, especially in complex components that require several tens or even hundreds of bends.

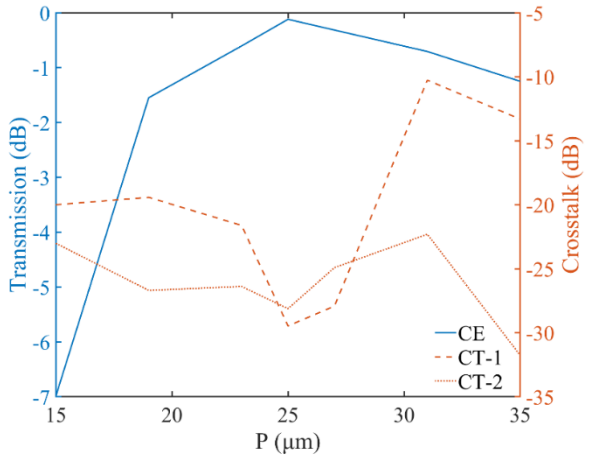

Figure S3 Simulated crosstalk when sweeping the parameter of the modulation period P. CE: coupling efficiency, CT: crosstalk.

Note 4: Bending loss

As light travels through a curved waveguide, the mode shifts toward the outer edge, leading to enhancement of losses due to increased interaction of the mode with the

sidewall surface roughness. In practice, the bending loss may be negligible if the radius of curvature is large; however, the propagation loss increases significantly at small radii. The modulation period P is strongly linked to the minimum bending radius given by Equation (2) and is, therefore, closely related to the propagation loss of AGF waveguides.

The radius of curvature of a parameterized curve is given by

$$R = \frac{1}{K} = \frac{(1+(y')^2)^{3/2}}{y''} \quad (S1)$$

For the sinusoidal profile $y = A\sin(\frac{2\pi}{P}t)$, we can get

$$R = \frac{P^2}{4\pi^2 A^2} \quad (S2)$$

As with other bent waveguides, the propagation loss generally increases when the bending radius of the waveguide decreases. For sinusoidal waveguides with an amplitude A = 0.53 μm and period P = 25 μm, the minimum bending radius is calculated to be 57 µm. The low-loss optical waveguides in this work, fabricated by the MPW foundry (LIGENTEC, Switzerland), exhibit a propagation loss of just 0.2 dB/cm. In standard Si_3N_4 single-mode waveguides, the minimum recommended bending radius with negligible bending loss is 50 μm, suggested by LIGENTEC, which is smaller than the minimum bending radius of the designed AGF-waveguide in this work.

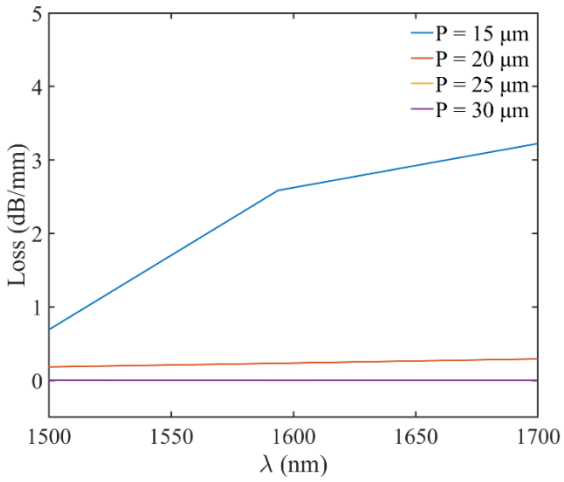

Figure S4 Simulated propagation loss of AGF waveguides with P varying from 15 μm to 30 μm (A is fixed at 0.53 μm). The yellow and purple lines of P = 25 μm and P = 30 μm overlap.

To verify this, the simulated loss of the AGF waveguides with the modulation

period varying from 15 μm to 30 μm is depicted in Fig. S4. Propagation loss measurements were made with the cut-back method. The simulation results show that the superlattice with the structural parameters used in this work introduces negligible loss. To investigate the transmission performance of AGF-enabled superlattices with a smaller modulation period of P = 20 μm, simulations in which the widths of the waveguide array change alternately from 1 μm to 1.15 μm are conducted. The optimized A and gap are 0.9 μm and 400 nm, and the transmission distance is set at 200 μm. The normalized field evolution and stimulated transmission spectra shown in Fig. S5 and Fig. S6 clearly demonstrate effective crosstalk suppression. However, this comes with higher propagation loss, reaching approximately 1.5 dB over a relatively short transmission distance of 200 μm.

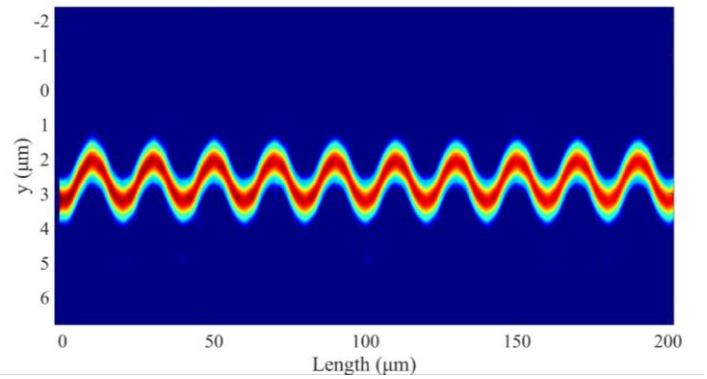

Figure S5 The normalized field evolutions of the AGF-enabled superlattices with P = 20 μm at 1550 nm (L = 200 μm, gap = 400 nm).

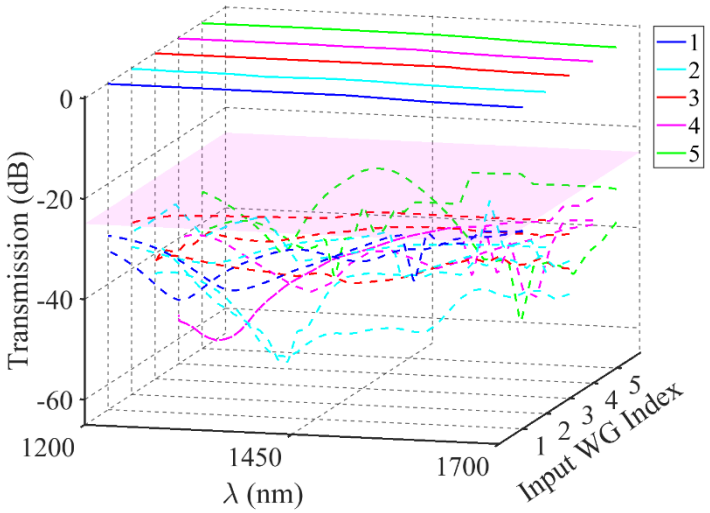

Figure S6 Simulated transmission spectra of binary superlattices with AGF (P= 20 μm, L = 200 μm, gap = 400 nm). The pink plane corresponds to −24 dB.

The experimental results of propagation loss across different waveguide configurations among 1 mm-long AGF samples, 1.5 mm-long AGF samples, and the straight waveguide have also been measured. There is no significant difference in propagation loss between the curved and straight waveguides. The propagation loss of AGF waveguides on the silicon nitride platform is negligible, confirming our analysis and aligning with results from the silicon-on-insulator (SOI) platform [16], [17], [12]. Additional loss on a SOI wafer due to curved nodes is about 0.61dB/cm, which is much smaller than the loss induced by sidewall roughness (3.91 dB/cm) [16]. In contrast, research indicates that the losses of the emerging lithium-niobate-on-insulator (LNOI) platform for a straight waveguide are approximately 0.53 dB/mm, while those for AGF waveguides are around 5.81 dB/mm [28]. Due to relatively immature fabrication techniques, the propagation loss of the LNOI structures is much higher because of the rough sidewall, limiting the potential photonic applications with AGF.

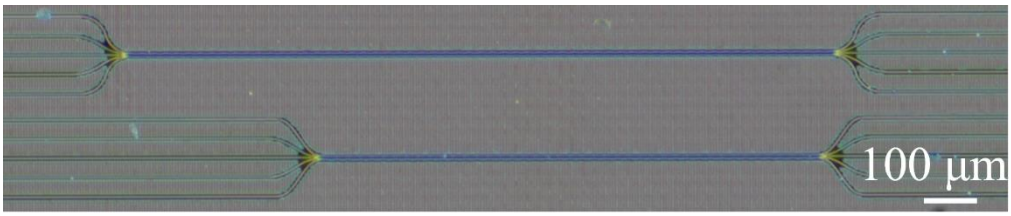

Figure S7 The microscope of the 1.5-mm long and 1-mm long AGF waveguides.

Note 5: Waveguide width

Crosstalk variation due to waveguide width changes has been simulated at gap widths of 400 nm and 500 nm, as shown in Fig. S8 and Fig. S9, respectively. Other structural parameters remain consistent with those used in this work, where A and P are optimized and fixed at 0.53 μm and 25 μm. The red squares in Fig. S8 and Fig. S9 indicate that most of the input light is coupled into the adjacent waveguide, resulting in a positive calculated value. The following points address the floating crosstalk caused by variations in waveguide width:

(1) Unlike conventional superlattices [15], significant differences in waveguide widths for AGF-enabled superlattices do not necessarily confine crosstalk to a small range.

(2) Increasing the separation between waveguides can significantly reduce crosstalk

while minimizing phase mismatch for certain structural parameters that suppress it.

(3) When the width fluctuates by 25 nm in AGF-enabled superlattices optimized for low crosstalk, the crosstalk remains low, as noted in the manuscript.

(4) As the spacing of the waveguide array increases, the tolerance for width variation improves further.

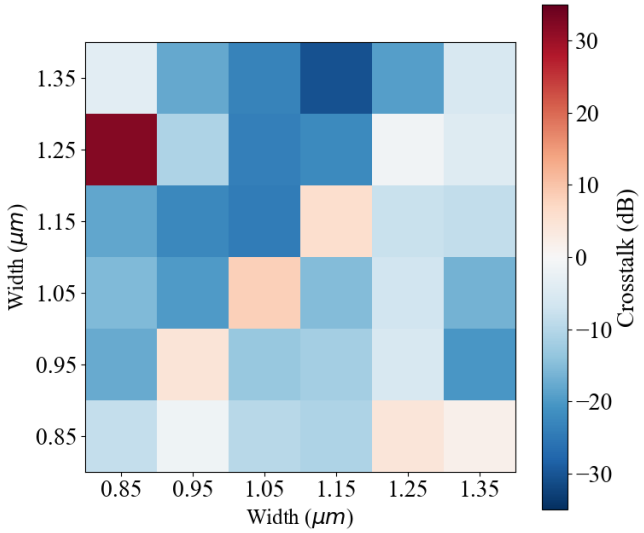

Figure S8 Stimulated crosstalk with width variation for a gap of 400 nm.

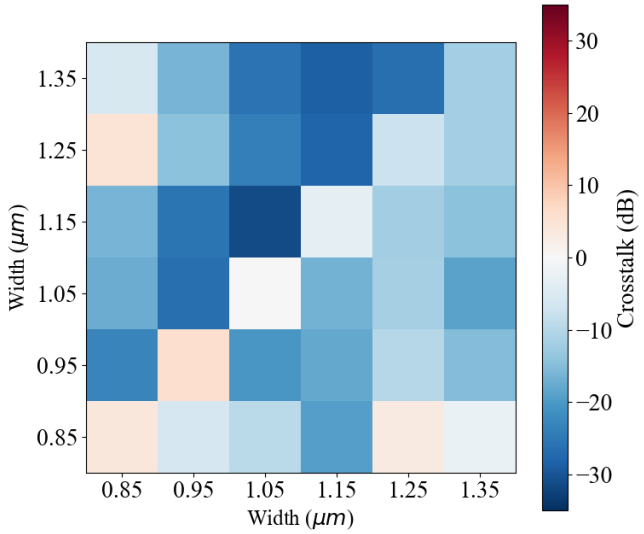

Figure S9 Stimulated crosstalk with width variation for a gap of 500 nm.

Note 6: Single-mode condition

To evaluate the single-mode condition, the width of the silicon nitride waveguide was

varied at 1550 nm. Fig. S10 illustrates the relationship between the waveguide width and the mode effective index. The width limit for the single-mode condition is 1.4 μm.

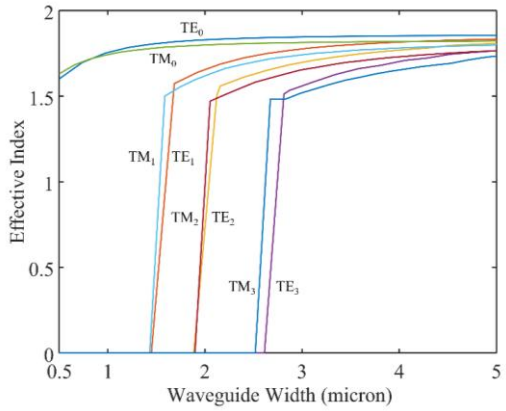

Figure S10 Simulated curves of effective refractive index for different waveguide widths.

Note 7: Design principles

The AGF-enabled superlattice combines two physical concepts: artificial gauge field [16], [17], and superlattice [12]. Therefore, its design principles also partially overlap with these two design methods. For AGF waveguides to achieve crosstalk suppression as described by Equation (3), the optimal amplitude of sinusoidal trajectory, A_{opt}, can be obtained. n_{eff} is the effective refractive index of a single waveguide with cross-sectional dimensions W and H. A and P are the amplitude and period of a sinusoidal waveguide, respectively.

$$A_{opt} = 2.405\frac{\lambda P}{4\pi^2(W+G)n_{eff}} \quad \text{(S3)}$$

The modulation period P is strongly linked to the minimum bending radius given by Equation (4) and is, therefore, closely related to the propagation loss of AGF waveguides. Due to the premise of AGF waveguides, P should be as small as possible [16]. The minimum bending radius with negligible loss is 50 μm advised by the MPW foundry (LIGENTEC, Switzerland). The reasonable modulation period is related to the inherent material properties and design rules of AGF waveguides. For the 220-nm silicon-on-insulator (SOI) platform, the modulation period of the AGF waveguide is 10 μm [17]. For this Si_3N_4 platform, P should be about 25 μm.

$$R = \frac{P^2}{4\pi^2 A^2} \quad \text{(S4)}$$

Based on Equations (3) and (4), the optimized AGF waveguides can be realized. The specific width variations, which are the basic element of the superlattice, should be introduced, considering the following factors [15]:

(1) The maximum waveguide width is constrained by the single-mode condition.

(2) Narrower waveguides lead to increased widths of optical modes, which can significantly enhance mode overlap between neighboring waveguides, thereby increasing mode coupling and propagation loss.

The band-gap diagram of the binary waveguide array needs to be computed, and the varying widths satisfying the n-"photon" resonances condition will be selected. Based on this platform, the widths of the waveguide arrays selected are 1300 nm, 1150 nm, 1000 nm, 850 nm, and 1400 nm. Finally, by fine-tuning the amplitude to get nearly zero coupling and a flat coupling dispersion within a specific broadband, the AGF-enabled superlattices towards colorless and low-crosstalk ultrahigh-density photonic integration can be realized.

Note that low crosstalk within broadband can be achieved using just two waveguide widths rather than relying on the complex width combination principles found in superlattice waveguides. In this work, multiple widths are employed solely to demonstrate the feasibility of integrating multi-width superlattices with artificial gauge fields. If the goal is to design an ultra-wideband, low-crosstalk waveguide array, alternating between just two widths with AGF is a quick and effective way.

Note 8: Experimental settings and DSP flows of 112Gbit/s data transmission

The experimental setup for the 112 Gbit/s PAM4 and discrete multi-tone (DMT) signal routing is shown in Fig. S11. A narrow linewidth tunable laser with an output wavelength set to 1550 nm served as the optical source. The light was externally modulated by a lithium niobate Mach-Zehnder modulator (MZM Optilab LCA-65) driven by the PAM4 signal, which was generated by an arbitrary waveform generator (AWG: Keysight 8195A) with a sample rate of 64 GSa/s. The signal was amplified by an electrical amplifier (EA) prior to driving the MZM. The MZM has a 3-dB electro-optical bandwidth of over 65 GHz and approximately 7-dB insertion loss. The

modulated optical high-speed signal was coupled to the on-chip waveguide through an edge coupler with a single-ended coupling loss of about 2.5 dB and then coupled into a lensed fiber and received by a photodetector (PD) with a 50-GHz bandwidth. The optical signal was coupled into the on-chip waveguide through an edge coupler using a lensed fiber and then received by ~~a photodetector (PD)~~ the PD. The received electrical signal was finally recorded by a real-time oscilloscope (RTO, Keysight Z592A) with a sample rate of 80 GSa/s for offline digital signal processing (DSP). At the transmitter side, the high-speed PAM4 signal was transmitted using a root-raised cosine (RRC) filter with a roll-off factor of 0.01 to compress the signal bandwidth. At the receiver side, a matched filter and a time-domain feed-forward equalizer (FFE) were applied to obtain lower bit error ratios (BERs). The launch power of the laser was large enough to ensure that the power of the optical signal received by the PD is maintained at about 1 dBm without using an erbium-doped fiber amplifier (EDFA). A pre-EDFA was employed before the PD only during the SNR test between different channels to compensate for the on-chip transmission loss and amplify the weak optical signal. To ensure consistency in the performance evaluation, the received optical power was set to be the same.

We implemented the DMT transmission to verify the ability of the proposed array to transmit high-order modulation formats. For the DMT signal modulation, a data rate of 112 Gbit/s is achieved with 160 subcarriers within a 32 GHz bandwidth. According to the signal-to-noise ratio response of the system, bit allocation is performed based on the Fischer algorithm. The original bit rate calculation formula for 112 Gbit/s is 517bits/330*64GSa/s=112 Gbit/s, where 517 is the total number of bits in one DMT symbol, 330 is the number of points in one DMT symbol, including 160 subcarriers and 10 cyclic prefixes, and one DMT symbol lasts 330/64ns.

In this proof-of-concept study, we primarily focused on end-to-end crosstalk measurements, due to design limitations. Specifically, the spacing of edge couplers is not designed according to the standard fiber array spacing used in the silicon nitride process, which prevented us from implementing the optical packaging necessary for multi-channel input testing. In our crosstalk and SNR measurements, we assumed that:

(1) Single-channel activation: The measurements were taken that only one input channel is active at a time.

(2) Minimal multi-channel influence: The inactive input channels have minimal impact on the active channels because simulation results show that the crosstalk between nearest neighbor waveguides is below -25 dB, consistent with the experimental results.

We measure the SNR profiles of the neighboring channels in Fig. S12 one by one because the edge coupler spacing is not designed according to the standard fiber array spacing of the silicon nitride process. chM-N represents the transmission when light is injected into I_M and detected from O_N. The SNR estimation process is achieved by sending a QPSK multi-tone probing signal to the AWG and measuring the error vector magnitude (EVM) of the received probing signal after the link transmission. The severely suppressed SNR between adjacent waveguides indicates that this dense waveguide array structure has excellent signal isolation and crosstalk suppression capabilities, which is critically important for reliable transmission in optical communication systems. This structure can allow each channel to operate independently without interference from neighboring channels.

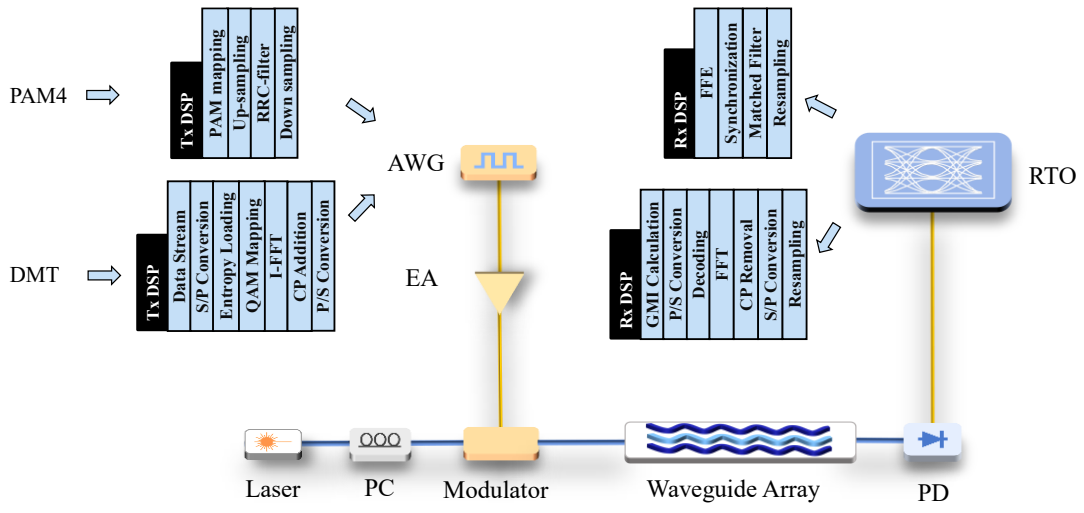

Figure S11 Experimental setup of the PAM4 and DMT data transmission. PC: polarization controller; EDFA: erbium-doped fiber amplifier; EA: electrical amplifier; AWG: arbitrary waveform generator; RTO: real-time oscilloscope; RRC: root-raised cosine; FFE: feed-forward equalization. P/S Conversion: parallel to serial conversion;

S/P Conversion: serial to parallel conversion; FFT: fast Fourier transform; I-FFT: inverse fast Fourier transform; QAM: quadratic amplitude modulation; CP: cyclic prefix.

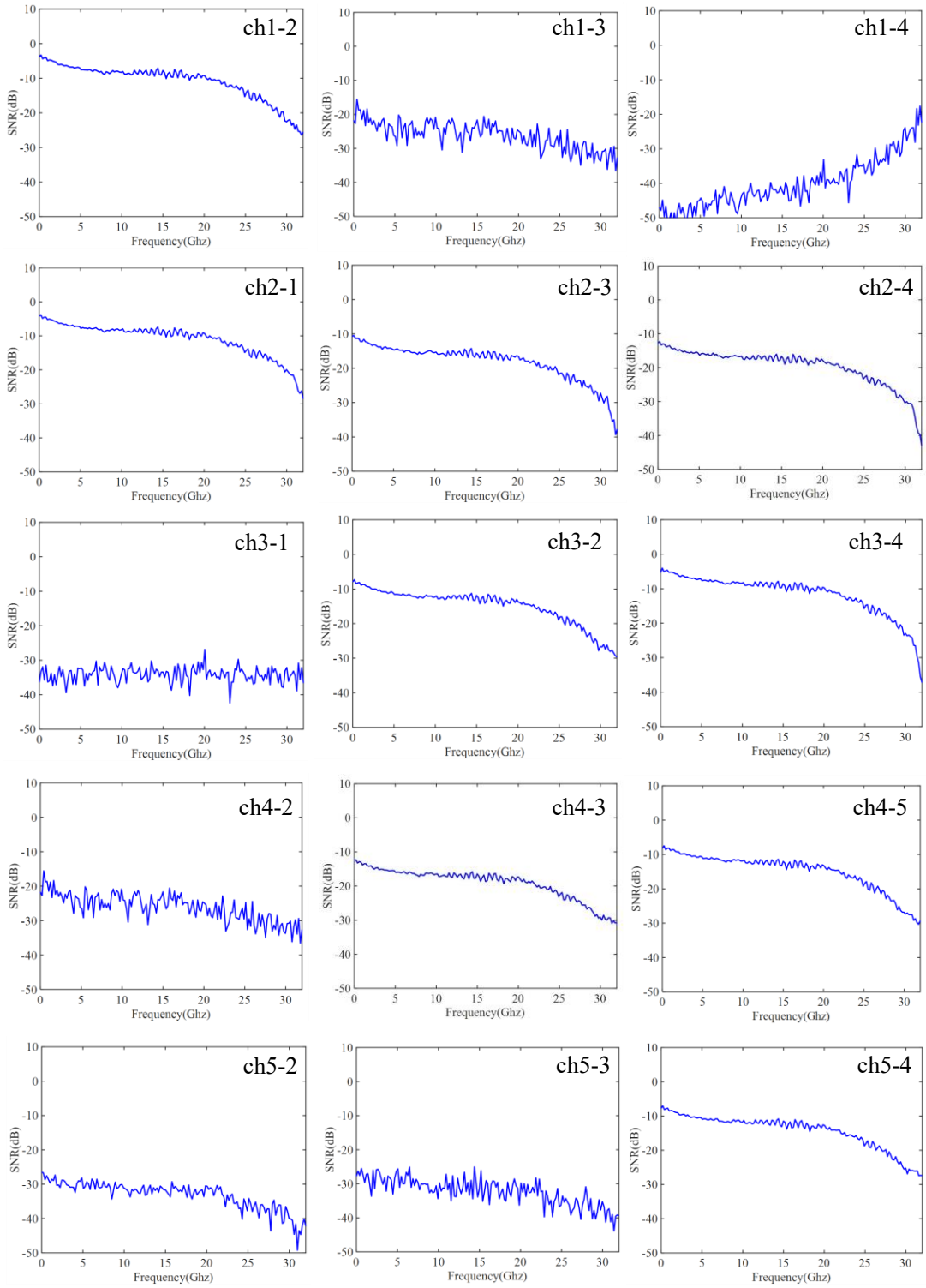

Figure S12 The SNR responses of the neighboring channels

The constellations of 32-QAM for 112 Gbit/s DMT signal under back-to-back and

on-chip transmission scenarios are shown in Fig. S13. The almost identical constellation diagrams after transmission compared to the BtB case indicate the superior signal quality of our designed device for transmitting high-order modulation formats.

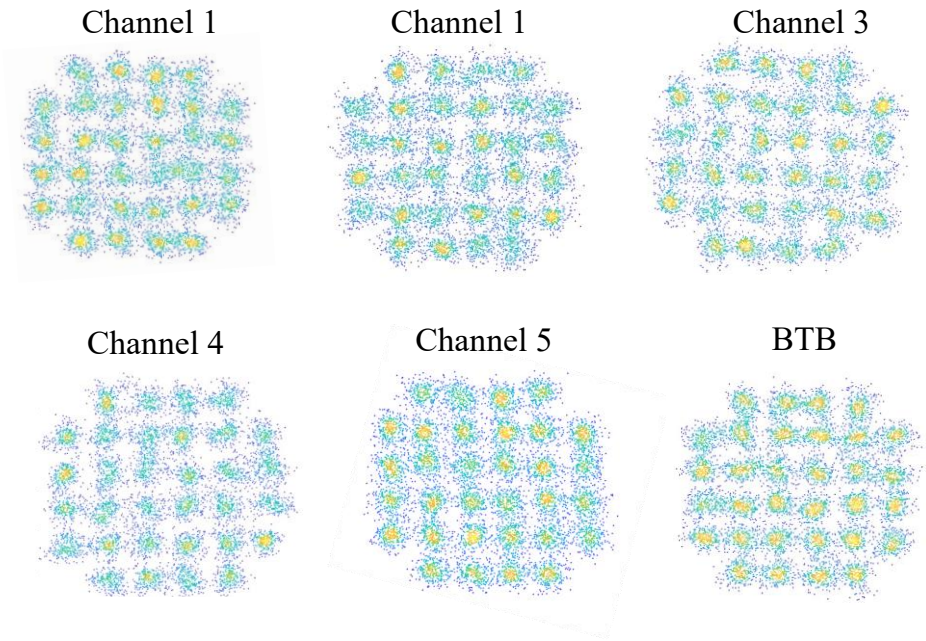

Figure S13 Constellation diagrams of the 32-QAM modulation for the 8th sub-carrier.

Besides, we conducted the high-speed 112 Gbit/s PAM4 signal transmission experiment through the AGF-enabled waveguide superlattice. Fig. S14 (a) and Fig. S14 (b) depict the bit error rate (BER) and eye diagrams after back-to-back (BtB) and five-channel transmission, respectively. The BER after transmission is below the 7\% HD-FEC threshold 3.8×10^{-3}. Thus, the ultra-compact signal routing of high-speed signals has been successfully achieved. The eye diagram in BtB transmission is clearly open, and we obtain almost the same eye diagrams after transmitting through the ultra-dense waveguides. The differences in the transmission performance due to insertion losses, crosstalk, or even environmental instability are roughly imperceptible compared with the BtB case.

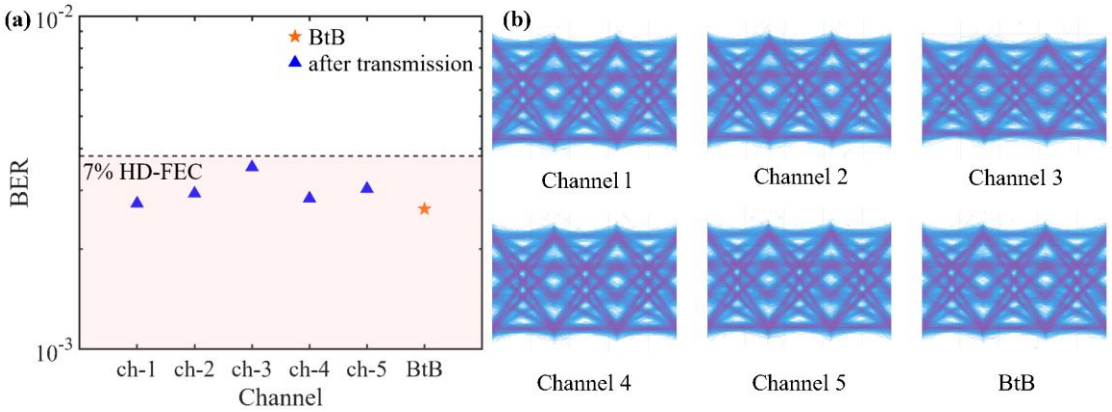

Figure S14 (a) The BER of 112 Gbit/s PAM4 after transmission through modulated samples. (b) Received eye diagrams of PAM4 signals.

TABLE S1 Performance comparison of crosstalk-reduction schemes in integrated photonics.

	Platform	Structure	Bandwidth(nm)	Polarization	Waveguide Structure(nm)	Cladding	Gap (nm)
This work	Si_3N_4 (n=1.97)	Superlattice with AGF	>500	TE&TM	1000×800	silica	400
[28]	LNOI (n=2.14)	Floquet engineering	>140	TE	900×300	air	1000
[14]	SOI (n=3.47)	Inverse design	<60	TE/TM	300×300	air	500
[17]		Artificial	<20	TE	500×220	air	195
[16]		gauge	~40	TE	500×220	air	250
[15]		bending	50	TE	500×220	air	270
[21]		Superlattice	320	TE	500×220	silica	500
[12]			>70	TE	500×220	air	280
[22]			30	TE&TM	400×340	air	400
[18]		Extreme-	N/A	TE	350×220	air	550
[19]		skin-depth	>80	TE	450×220	air	550
[20]		Adiabatic elimination	N/A	TE	275×340	air	720

[a]Bandwidth is defined as the wavelength range where crosstalk is below −20 dB. Some studies actually have wider bandwidths but have not been fully demonstrated, so we denote them with ">".

[b]The refractive indices of the materials are given. The pitches and widths of single-mode Si_3N_4 and LNOI waveguides are larger than those of SOI waveguides because of their low refractive index.

It is seen in Table S1 that the advanced waveguide array design concept reported in this work has a very broad bandwidth supporting dual polarizations, in comparison with other approaches. The gap between the waveguides is also extremely small when considering the wide width of the single-mode waveguide and the small refractive index difference between silicon nitride and silicon oxide cladding.

Note 9: Measurement Setup

The measurement setup is shown in Fig. S15. We used a broadband light source (SuperK, NKT Photonics) and an optical spectrum analyzer (OSA, Yokogawa AQ3670D) to characterize the device. Input light with a wavelength of 1200 nm to 1700 nm was coupled into the device through an edge coupler. The output signal was first collected by a polarization-maintaining lensed fiber and then sent to the OSA to get the transmission spectra.

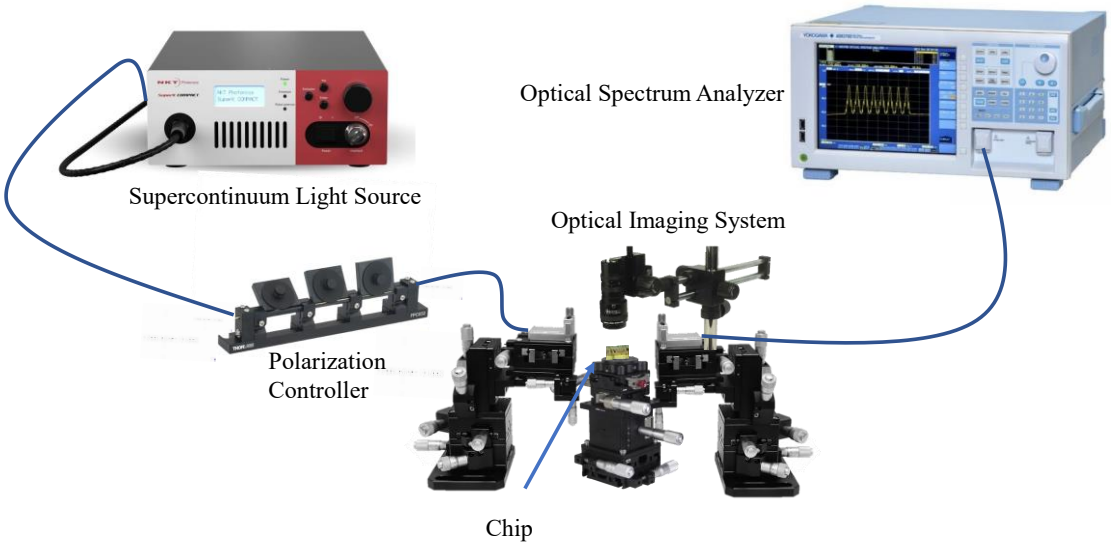

Figure S15 Schematic of the measurement setup.

Note 10: Design and fabrication of the Si_3N_4 waveguide array

The ultra-low-loss waveguide was fabricated on an 800-nm-thick Si_3N_4 layer, deposited by low-pressure chemical vapor deposition (LPCVD) by Ligentec. The thickness of the top oxide and the bottom oxide are 6.6 μm and 4.0 μm, respectively.